JACS
JOURNAL OF THE AMERICAN CHEMICAL SOCIETY
Article
pubs.acs.org/JACS

A New Molecular Design Based on Thermally Activated Delayed Fluorescence for Highly Efficient Organic Light Emitting Diodes

Pachaiyappan Rajamalli,[†] Natarajan Senthilkumar,[†] Parthasarathy Gandeepan,[†] Pei-Yun Huang,[†] Min-Jie Huang,[†] Chen-Zheng Ren-Wu,[‡] Chi-Yu Yang,[‡] Ming-Jui Chiu,[†] Li-Kang Chu,[†] Hao-Wu Lin,[‡] and Chien-Hong Cheng*[,†]

[†]Department of Chemistry, National Tsing Hua University, Hsinchu 30013, Taiwan

[‡]Department of Materials Science and Engineering, National Tsing Hua University, Hsinchu 30013, Taiwan

Supporting Information

ABSTRACT: Two benzoylpyridine-carbazole based fluorescence materials DCBPy and DTCBPy, bearing two carbazolyl and 4-(*t*-butyl)carbazolyl groups, respectively, at the *meta* and *ortho* carbons of the benzoyl ring, were synthesized. These molecules show very small ΔE_{ST} of 0.03 and 0.04 eV and transient PL characteristics indicating that they are thermally activated delayed fluorescence (TADF) materials. In addition, they show extremely different photoluminescent quantum yields in solution and in the solid state: in cyclohexane the value are 14 and 36%, but in the thin films, the value increase to 88.0 and 91.4%, respectively. The OLEDs using DCBPy and DTCBPy as dopants emit blue and green light with EQEs of 24.0 and 27.2%, respectively, and with low efficiency roll-off at practical brightness level. The crystal structure of DTCBPy reveals a substantial interaction between the *ortho* donor (carbazolyl) and acceptor (4-pyridylcarbonyl) unit. This interaction between donor and acceptor substituents likely play a key role to achieve very small ΔE_{ST} with high photoluminescence quantum yield.

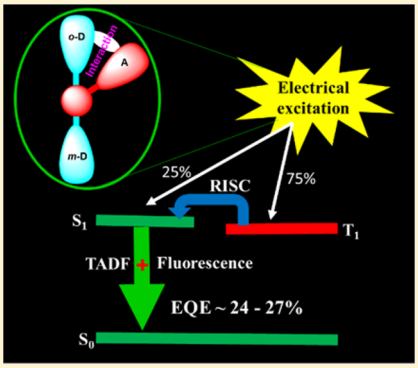

INTRODUCTION

OLED displays possess many performance advantages over LCD including wider viewing angles, higher contrast ratio, faster response times, access to flexible panels, high luminous efficiency, facile color tuning of emitters and lighter weight.[1−9] In the past few decades, intensive research in OLEDs has successively led to improved fluorescent and phosphorescent emitters for the devices.[10−17] For common fluorescent emitters, the radiative decay of triplet excitons (75%) is spin forbidden, and only singlet excitons (25%) can be recruited to produce light. Conversely, noble metal based organophosphor complexes exhibit emissive triplet states due to singlet−triplet state mixing via efficient spin orbit coupling, and thus they can harvest both singlet as well as triplet excitons (100%) for emission.[18,19] Although phosphorescent emitters produce devices with high efficiencies, the requirement of expensive noble metals and the short operation lifetime of blue emission device remain problematic for practical applications.

Recently, organic delayed fluorescence materials including those that show triplet−triplet annihilation (TTA) and thermally activated delayed fluorescence (TADF) properties have been considered as dopants for highly efficient OLEDs.[20−23] However, OLEDs based on TTA materials are limited to an internal quantum efficiency of only 62.5%.[24] On the other hand, TADF materials have arisen as an inexpensive alternatives to high-performance phosphorescent noble metal complexes for OLEDs.[25−32] In principle, TADF originates from charge transfer (CT) systems with a thermally accessible gap between the lowest singlet (S_1) and triplet (T_1) excited states, that enable the harvest of both singlet and triplet excitons under electrical excitation.[33] It is realized in molecules with a small overlap between their highest occupied molecular orbital (HOMO) bearing donor units and lowest unoccupied molecular orbital (LUMO) bearing acceptor units. Although significant efforts have been taken for the development of new TADF emitters, few of TADF-based devices display external quantum efficiency (EQE) similar to those using noble metal complexes as the emitters.[34−39] TADF molecules in nature possess trade-off between the efficiency of RISC (T_1 to S_1) and singlet to ground state (S_1 to S_0) radiative decay. The RISC, in general, increases with decreasing ΔE_{ST} and the best approach to minimize ΔE_{ST} is to separate the spatial distribution of HOMO and LUMO[36] by increasing the twist angle between the donor and acceptor planes of the molecule. However, a large twist angle generally suppresses the S_1 to S_0 radiative decay and leads to decrease of the radiative efficiency.

Hence, the search for TADF emitters with efficient RISC and also with very high fluorescence efficiency to achieve efficient TADF device are highly desired. An alternative option to reduce the ΔE_{ST} by through intramolecular space interaction between donor and acceptor.[40] Herein, we designed and

Received: October 20, 2015
Published: December 28, 2015

DOI: 10.1021/jacs.5b10950
J. Am. Chem. Soc. 2016, 138, 628−634

synthesized two donor−acceptor−donor (D-A-D) molecules, 2,5-di(9*H*-carbazol-9-yl)phenyl)(pyridin-4-yl)methanone (DCBPy) and (3,5-bis(3,6-di-*tert*-butyl-9*H*-carbazol-9-yl)-phenyl)(pyridin-4-yl)methanone (DTCBPy), for application as TADF emitters in OLEDs. In these molecules, a new acceptor phenyl(pyridin-4-yl)methanone was introduced and the two carbazole donors are *ortho* and *meta* connected to the phenyl ring of the acceptor. These molecules show very small ΔE_{ST} (0.03−0.04 eV) with very high photoluminescent efficiencies. In addition, their transient PL characteristics reveal clearly the TADF property and the use of these two emitters for green and blue OLEDs gives very high external quantum efficiency (EQE) of 27.2% and 24.0% with low turn-on voltage and reduced roll-off. Strong intramolecular space-interaction between donor and acceptor opens up a new possibility to achieve efficient TADF emitters and the TADF material-based OLEDs.

RESULT AND DISCUSSION

Synthesis and Physical Properties. Synthesis route for DCBPy and DTCBPy were shown in Scheme 1. These materials can be easily synthesized in two steps via bromination of benzoylpyridine by NBS, and then *N*-carbazolylation using inexpensive Cu as the catalyst.

Scheme 1. Synthesis of DCBPy and DTCBPy

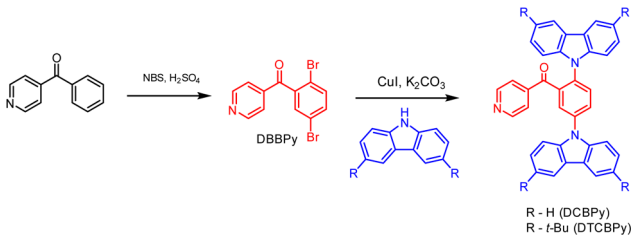

The detailed synthesis procedures and chareterizations are given in the Experimental Section and Supporting Information. The compounds were purified by temperature gradient vacuum sublimation and characterized by ^{1}H, and ^{13}C NMR, single crystal analysis and high resolution mass spectrometry. The crystal structure of DTCBPy confirms the proposed structure with the two donor *t*-butyl carbazole groups are *para* to each other and positioned at the *ortho* and *meta* to the pyridine carbonyl moiety. The *ortho t*-butyl carbazole group shows strong intramolecular space interaction with acceptor unit with a distance of 2.9−3.7 Å (Figure 1). The observed distances suggest that a significant intramolecular interaction exists between these two nearly parallel planes. The presence of keto group in the molecule increases the electron accepting ability of the benzoylpyridine unit and also help to arrange a better interaction between the *ortho* carbazolyl and pyridoyl groups.

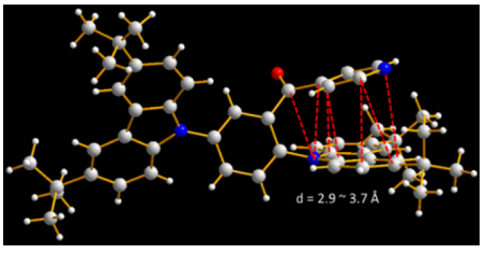

Figure 1. Crystal structure of DTCBPy.

These molecular designs are guided by the time dependent density functional theory (TDDFT) calculations to find HOMO−LUMO separation and ΔE_{ST} values. As depicted in Figure 2, the HOMOs of DCBPy and DTCBPy are mainly

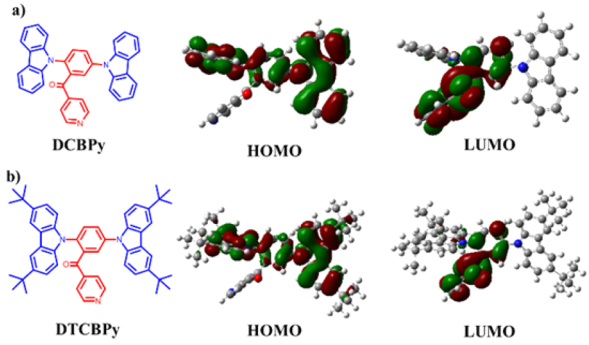

Figure 2. Structures and molecular orbitals of (a) DCBPy and (b) DTCBPy.

distributed over the two carbazolyl groups and slightly extended to the phenyl ring. The LUMOs are mostly localized on the BPy core and slightly extended to the phenyl ring, based on the TDDFT calculation. There is a small degree of spatial overlap between the HOMO and LUMO in these two molecules. It is noteworthy that the small spatial overlap is important for high luminescence efficiency of the molecule.[36] Moreover, the TDDFT calculation shows small singlet and triplet energy gaps (ΔE_{ST}) of 0.11 and 0.10 eV for DCBPy and DTCBPy, respectively. The intramolecular space interaction was also observed between *ortho*-donor and acceptor from DFT calculation (Figure S1), but the distance between the *ortho t*-butyl carbazolyl and pyridoyl groups is slightly larger than the value measured from the results of single crystal X-ray diffraction (Figure 1). Notably, the *meta* and *ortho* carbazoles are para to each other and a strong electronic interaction between these two groups leading to a stronger donating ability are expected. The *meta* carbazole plays a role in dispersing the HOMO, it is known that a widely dispersed HOMO enhances the efficiency compared with the less dispersed one and also improve the thermal stability of these materials.

The absorption and emission spectra of DCBPy and DTCBPy in various solvents are shown in Figure S2 and summarized in Table 1. DCBPy in all solutions exhibits a broad absorption band at 400 nm, assigned to the CT absorption associated with the electron transfer from the carbazole groups to the benzoylpyridine moiety. Similar absorption band centered at 418 nm was also observed for DTCBPy. No significant change was observed of the absorption spectra in various solvents for both compounds. Conversely, DCBPy displays a significant positive solvatochromic effect of its fluorescent emission in different solvents from blue (477 nm) in *n*-hexane to yellow (560 nm) in dichloromethane (Figure S2). Similarly, the emission of DTCBPy shifts from 478 nm in hexane to 561 nm in DCM. The phosphorescent emission spectra of DCBPy and DTCBPy, taken at 77 K in toluene (10^{-5} M) are also in Figure 3a showing peaks centered at 495 and 509 nm, respectively. The triplet energies were calculated to be 2.84 and 2.70 eV from the onset of their phosphorescence spectra. DCBPy and DTCBPy in toluene at room temperature show fluorescence peaks centered at 490 and 508 nm, respectively

DOI: 10.1021/jacs.5b10950
J. Am. Chem. Soc. 2016, 138, 628−634

Table 1. Physical Properties of DCBPy and DTCBPy

dopant	λ_{abs} (nm)[a]	λ_{em} (nm)[a]	λ_{em} (nm)[b]	λ_{em} (nm)[c]	T_g (°C)[d]	T_d (°C)[e]	HOMO (eV)[f]	LUMO (eV)[g]	E_g (eV)[h]	E_T (eV)[i]
DCBPy	311, 400	490	514	495	109	382	−5.75	−2.88	2.87	2.84
DTCBPy	320, 418	508	518	509	140	412	−5.61	−2.87	2.74	2.70

[a]Measured in toluene (1×10^{-5} M) at room temperature. [b]Measured in thin film at room temperature. [c]Phosphorescence measured in toluene (1×10^{-5} M) at 77 K. [d]Obtained from DSC measurements. [e]Obtained from TGA measurement. [f]Measured from the oxidation potential in 10^{-3} M DCM solution by cyclic voltammetry. [g]Measured from HOMO − E_g. [h]Estimated from the onset of fluorescence spectrum. [i]Estimated from the onset of phosphorescence spectrum.

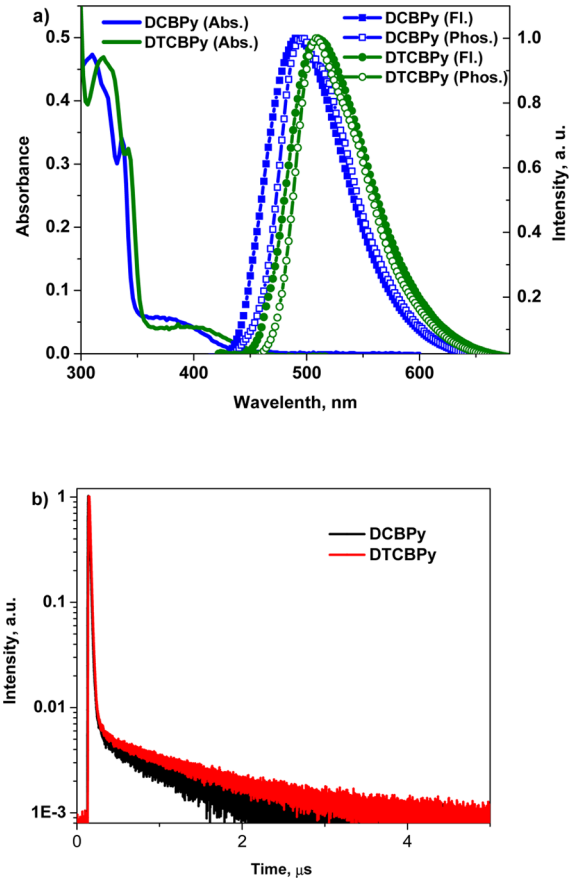

Figure 3. (a) Absorption (Abs.) and fluorescence (Fl.) spectra in toluene (10^{-5} M) solution at room temperature and phosphorescence (Phos.) spectra in toluene (10^{-5} M) at 77 K; and (b) their transient PL characteristics in toluene (10^{-5} M) at room temperature under vacumm.

and their singlet energies calculated from the onset of fluorescence spectra are 2.87 and 2.74 eV as summarized in Table 1. The ΔE_{ST} was estimated to be 0.03 eV for DCBPy and 0.04 eV for DTCBPy based on the onset calculation and comparable with the reported TADF materials.[34] Comparison of the calculated and experimental E_g, E_T and ΔE_{ST} values are summarized in Table S1. The small ΔE_{ST} of these two molecules indicate that they plausibly possess TADF property with efficient up-conversion from T_1 to S_1.

The electrochemical properties of DCBPy and DTCBPy were investigated by cyclic voltammetry (Figure S3). From the oxidation and reduction waves of these two compounds obtained from the voltamograms (Figure S3). The HOMO levels were calculated to be −5.75 and −5.61 eV for DCBPy and DTCBPy, respectively and the values are obtained based on onset of the oxidation potentials and the ionization potential (4.8 eV) of Fc/Fc+. The LUMO energy levels were estimated from HOMO − E_g to be −2.88 and −2.87 eV. To check the electrochemical stability of these materials, we studied the electrochemical behaviors under repeated CV scans. As shown in Figure S4, DTCBPy showed reversible oxidization with no change of the oxidation potentials after 19 repeated scans. This observation indicates that the DTCBPy cation is stable in the solution. However, the oxidation potentials of DCBPy shift gradually to lower values during the repeated CV scans indicating that DCBPy is electrochemically less stable than DTCBPy due to the known more electrochemical active sites C3 and C6 (para to the nitrogen) of the carbazole groups in DCBPy.[41]

Further, to know the PL stability of these materials, we studied the UV-induced degradation behavior of the thin films of these materials. The samples consisting of ITO/DTCBPy or DCBPy (80 nm) were fabricated and encapsulated under nitrogen. The samples were continuously exposed to 340 nm illumination and their PL spectra were recorded once every hour and were shown in Figure S5. A comparison of the spectra in Figure S5 revealed that DTCBPy is more stable than DCBPy under UV irradiation. There is no detectable change of the DTCBPy PL spectra after 10 h exposure, but a slow decaying was observed for the DCBPy thin film. Thus, both electrochemical and UV irradiation measurements suggest that DTCBPy is more stable than DCBPy. Stability of these films under electrical stress would be similar to the PL stabilities. Hence, the photochemical stability of these material toward excitons in devices can be assessed by the UV-degradation behavior of their films.[42] In oxygen-free cyclohexane, the quantum yields are 14% and 36%, respectively for DCBPy and DTCBPy. In the presence of oxygen the values decrease to 5% and 11.4%. The decrease of photoluminescence quantum efficiencies of these compounds in the presence of oxygen also supports that these two molecules possess TADF property[25] and the T1 states of these molecules, which are readily quenched by the triplet ground state oxygen molecules, undergo reverse intersystem crossing (RISC) from T1 to S1.[43] The quench of T1 by oxygen leads to the quench of delayed fluorescence and the decrease of the fluorescence intensity. The photoluminescence quantum efficiencies of these molecules in various solvents were also measured and summarized in Table S2.

In addition, the fluorescence and phosphorescence spectra of the doped films (CzPS: DCBPy (5 wt %) and CBP: DTCBPy (5 wt %)) were measured (Figure S6) and the ΔE_{ST} is 0.07 and 0.08 eV, respectively; the values were determined from the onset of the fluorescence and the phosphorescence spectra. The PL and phosphorescence spectra for DTCBPy crystals were also measured and are shown Figure S6c. Based on these spectra, a ΔE_{ST} (0.08 eV) was obtained. The value is close to that of the codoped (CBP:DTCBPy) thin film indicating that the molecular conformation in the single crystals and codoped thin film is similar. PL quantum yields (PLQY) of the doped

DOI: 10.1021/jacs.5b10950
J. Am. Chem. Soc. 2016, 138, 628−634

films also were measured and were listed in Table S2. The absolute PLQYs of the CzPS: DCBPy and CBP: DTCBPy films were 88.0 and 91.4%, respectively, much higher than those in solutions. This PL quantum yield enhancement is due to the suppression of collisional and intramolecular rotational quenching in the solid state.[25,44] Moreover, the crystal structure also clearly shows a substantial interaction between the ortho carbazole and benzoylpyridine units (Figure 1) further increasing the rigidity of the molecules and enhancing the PL quantum yields in the solid state (crystals and thin films). Unlike most of the reported TADF molecules, the present molecular design provides small ΔE_{ST} but with adequate overlap between HOMO and LUMO for enhancing RISC and S_1 to S_0 (radiative), respectively.[25]

The transient PL decay characteristics of these two materials were measured in 10^{-5} M toluene solution under vacuum and are shown in Figure 3b. As shown in the Figure 3b, each of the transient decay curves can be divided into two components. The first one is the prompt emission decay curve from S_1 to ground state (S_0); the lifetime (τ) of the emission calculated from intensity vs time is 15 and 18 ns for DCBPy and DTCBPy, respectively. The second one is a delayed emission component with τ = 0.6 and 1.0 μs for DCBPy and DTCBPy, respectively; these delayed emissions may be rationalized as the thermal up-conversion of T_1 to S_1, followed by fluorescence to the ground state. The short excited state lifetime of these molecules are comparable with highly emissive phosphorescent iridium complexes. The short delayed emission lifetimes with high PL quantum yields in the solid state of these two materials are an important feature of TADF emitter to realize high device efficiencies. Further, to confirm the TADF property, temperature dependent transient PL measurements are carried out for the doped film, DCBPy (5 wt %):CzPS at temperatures between 100 to 300 K. As shown in Figure 4, the intense

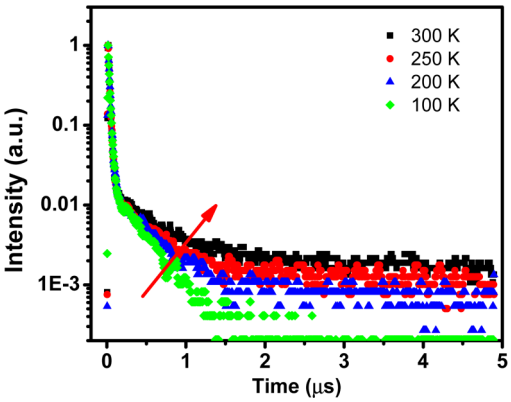

Figure 4. Temperature dependent transient PL characteristics of 5 wt % DCBPy doped in CzPS film and measured using 355 nm pulsed laser.

emission and long tail are from prompt and delayed fluorescence, respectively. The delayed emission component gradually increase with increase of temperature from 100 to 300 K. It reveals that the T_1 to S_1 up-conversion increases with increasing temperature. The results further support that DCBPy is TADF material.[43] Most of the reported TADF materials shows high up-conversion at 250 K and reduced at 300 K due to nonradiative decay at higher temperature.[45,46] Unlike reported materials, DCBPy show high up-conversion even at 300 K.

The thermal properties of these emitters were determined by thermogravimetric analysis (TGA) and differential scanning calorimetry (DSC) under nitrogen atomosphere and the results are shown in Figures S7 and S8. Both DCBPy and DTCBPy showed very high thermal stability with decomposition temperatures (T_d) of 382 and 412 °C and glass transition temperatures (T_g) of 110 and 140 °C. The introduction of tertiary butyl groups to the carbazole moieties appears to increase the T_g and T_d of DTCBPy by 30 °C relative to those of DCBPy. The high thermal values endow high morphologic stability of the amorphous phase in the film.

Device Fabrication. To investigate the electroluminescence properties of DCBPy and DTCBPy, multilayer OLEDs was fabricated using DCBPy and DTCBPy doped films as the emitting layers (EML). Device B is constructed using DCBPy as the dopant with the device structure: ITO/NPB (30 nm)/*m*CP (20 nm)/CzPS: DCBPy (5%) (30 nm)/DPEPO (5 nm)/TmPyPb (60 nm)/LiF (1 nm)/Al (100 nm). In this device, *N*,*N*′-bis(1-naphthyl)-*N*,*N*′-diphenyl-1,1′-biphenyl-4,4′-diamine (NPB) acts as a hole injection material, *m*CP as a hole-transporting material and also as an exciton blocker to prevent exciton diffusion to the NPB layer, while 9,9′-(sulfonylbis(4,1-phenylene))bis(9*H*-carbazole) (CzPS) is a host material, 1,3,5-tri(m-pyrid-3-yl-phenyl)benzene (TmPyPb)[47,48] is the electron-transporting material and oxybis(2,1-phenylene))bis-(diphenylphosphine oxide (DPEPO) is an exciton blocker.[33] Device G is fabricated using DTCBPy as the dopant with the device structure: ITO/NPB (30 nm)/TAPC (20 nm)/CBP: DTCBPy (5%) (30 nm)/PPT (10 nm)/TmPyPb (55 nm)/LiF (1 nm)/Al (100 nm), where 1,1-bis[4-[*N*,*N*′-di(ptolyl)amino]-phenyl] cyclohexane (TAPC) acts as a hole-transporting material, 4,4′-bis(*N*-carbazolyl)-1,1′-biphenyl (CBP) as a host material and dibenzo[*b*,*d*]thiophene-2,8-diylbis-(diphenylphosphine oxide) (PPT) as an exciton blockers. The structures of the compounds and schematic representation of device structure are shown in Figure 5.

The electroluminescent properties of these two devices are displayed in Figure 6, Figure S9 and summarized in Table 2.

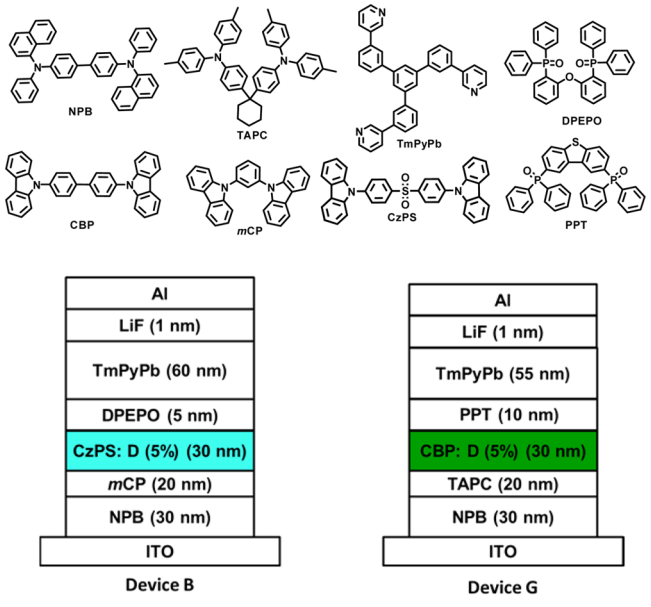

Figure 5. Structures of the materials used in devices and schematic representation of device B and G.

DOI: 10.1021/jacs.5b10950
J. Am. Chem. Soc. 2016, 138, 628−634

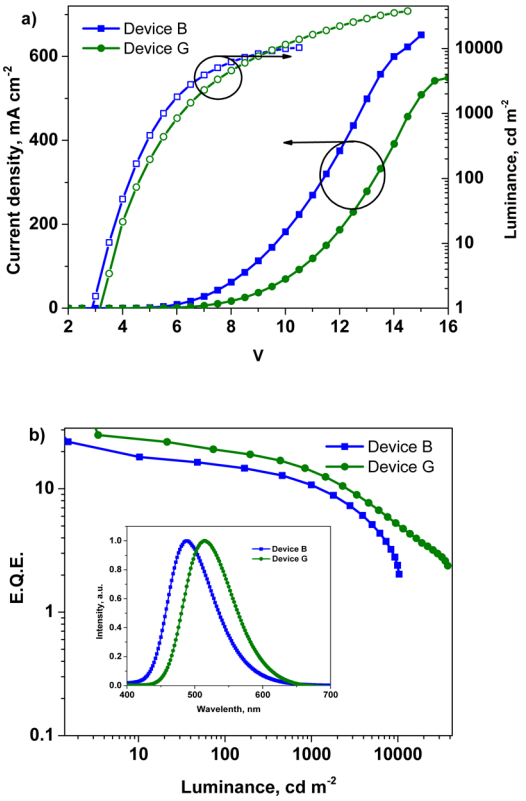

Figure 6. EL characteristic plots of devices B and G: (a) current density and luminance vs driving voltage, (b) external quantum efficiency vs luminance and inset: electroluminescent spectra.

Device B gave sky blue electroluminescence with a low turn on voltage of 2.8 V and CIE (0.17, 0.36).[49,50] Besides, a maximum external quantum efficiency, current efficiency, and power efficiency of 24.0%, 54.7 cd A^{-1}, and 57.2 lm W^{-1}, respectively, were achieved. These efficiencies are comparable to those of blue phosphorescent OLEDs.[49,50] Device G based on DTCBPy emitted green light with CIE (0.30, 0.64) and exhibited a maximum external quantum efficiency, current efficiency, and power efficiency of 27.2%, 94.6 cd A^{-1}, and 84.7 lm W^{-1}, respectively. These efficiencies are also comparable to those of the iridium-based green phosphorescent OLEDs.[49,50] The electroluminescent spectra of devices B and G were measured at various voltages. Figure S10 indicates that there is no noticeable change in the EL spectra even at high operating voltage. Devices B and G showed maximal luminance up to 10300 and 37700 cd m^{-2} at 10.5 and 14.5 V in the absence of light out-coupling enhancement. These device efficiencies are much higher than most of the reported devices based on TADF emitters. This result suggest that, efficient TADF emitters can be achieved by this new intramolecular space interaction approach found to be an ideal method to get extremely efficient TADF materials.

To compare the device performances with well-known green phosphorescent emitter tris[2-phenylpyridinato-C^2,N]iridium-(III) ($Ir(ppy)_3$), device G1 was fabricated with the device structure similar to that of G and the results are shown in Figure S11 and summarized in Table 2. The device performance is comparable with the reported values.[51] It is noteworthy that the DTCBPy-based device G shows better performance than G1 does at low brightness, although the latter becomes better at higher brightness due to the larger efficiency roll-off of G (see Table S3).

The observed high device efficiencies suggest very efficient thermal up-conversion of triplet excitons T_1 to S_1 and highly fluorescent efficiency (S_1 to S_0, vide supra) of the two dopants DCBPy and DTCBPy in the devices. External quantum efficiencies and current efficiencies of devices B and G at brightness of 100 cd m^{-2} and 1000 cd m^{-2} were summarized in Table S3. Notably, device G also shows relatively reduced roll-off compared to other TADF devices; at a brightness level of 100 cd m^{-2} and 1000 cd m^{-2}, the external quantum efficiencies still retain as high as 20.5% and 14.0%, respectively. We attribute the results to the small ΔE_{ST} and suppressed nonradiative decay at high brightness level.[34]

Furthermore, to confirm the TADF property in the device, the transient electroluminescence was measured for device B at room temperature. Figure 7 shows that the delayed electroluminescence component lasts for several tens of microseconds with a very high delayed component to prompt ratio. The result indicates that the EL efficiency is mostly contributed by the delayed fluorescence, supporting the importance of TADF process in the device. In contrast to the transient EL characteristics, the delayed fluorescence component of the

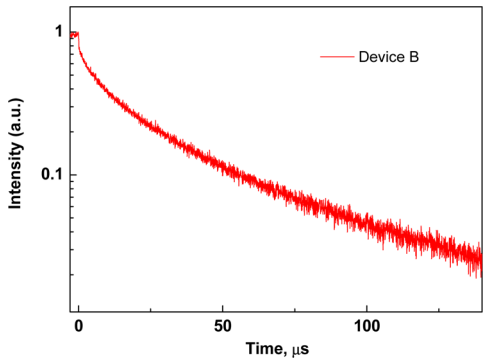

Figure 7. Transient electroluminescence characteristics of device B measured at 3 V.

Table 2. EL Performances of the Devices Using DCBPy, DTCBPy and $Ir(ppy)_3$ as Dopants[a,b]

device	V_d (V)	L (cd m^{-2}, V)	EQE (%, V)	CE (cd A^{-1}, V)	PE (lm W^{1-}, V)	λ_{max} (nm)	CIE (x,y), V
B	2.8	10300, 10.5	24.0, 3.0	54.7, 3.0	57.2, 3.0	488	(0.17, 0.36), 8
G	3.1	37700, 14.5	27.2, 3.5	94.6, 3.5	84.5, 3.5	514	(0.30, 0.64), 8
G1	2.54	71000, 14.0	24.5, 3.5	85, 3.5	76, 3.5	512	(0.28, 0.60), 8

[a]Device configuration for B: ITO/NPB (30 nm)/*m*CP (20 nm)/CzPS: DCBPy (5 wt %) (30 nm)/ DPEPO (5 nm)/ TmPyPb (60 nm)/LiF (1 nm)/Al (100 nm) and for G and G1: ITO/NPB (30 nm)/TAPC (20 nm)/CBP: DTCBPy or $Ir(ppy)_3$ (5 wt %) (30 nm)/PPT(10 nm)/ TmPyPb (55 nm)/LiF (1 nm)/Al (100 nm), respectively. [b]V_d, The operating voltage at a brightness of 1 cd m^{-2}; L, maximum luminance; EQE, maximum external quantum efficiency; CE, maximum current efficiency; PE, maximum power efficiency; and λ_{max}, the wavelength where the EL spectrum has the highest intensity.

DOI: 10.1021/jacs.5b10950
J. Am. Chem. Soc. 2016, 138, 628−634

transient PL characteristics (Figure 4) is relatively weak indicating that the radiative decay of singlet excitons from S_1 to S_0 is predominant relative to the ISC from S_1 to T_1. Therefore, a weak TADF and strong prompt fluorescence were obtained in the PL process. Conversely, the TADF process dominates the device emission under electrical excitation and this efficient RISC from T_1 to S_1 leads to intense delayed fluorescence, which contributes to the high EL efficiency of this OLED.

CONCLUSION

In summary, we have designed and synthesized TADF emitters DCBPy and DTCBPy bearing a new benzoylpyridine core as an electron-accepting unit and two carbazolyl, *t*-butyl carbazolyl groups as the electron-donating units. These two emitters exhibit the requisite properties for TADF materials including very small ΔE_{ST}, transient PL decay curves with a normal and a delayed fluorescent component, and reduced PL efficiency in the presence of oxygen. Substantial intramolecular interaction between the donor and adjacent acceptor units play an important role in displaying efficient TADF properties. The OLEDs using DCBPy and DTCBPy as the emitter achieved maximum EQE values of 24.0% and 27.2% respectively, with relatively low efficiency roll-off at practical brigthness and are among the best performance TADF-based OLEDs. These new approach in molecular design open up the possibility of achieving potentially promising TADF emitters for the applications in the future organic flat panel display and lighting.

EXPERIMENTAL SECTION

Synthesis of (2,5-dibromophenyl)(pyridine-4-yl)methanone (DBBPy). To a stirred solution of 4-benzoylpyridine (6.00 g, 32.8 mmol) in conc. H_2SO_4 (20 mL) at 60 °C, NBS (14.0 g, 78.7 mmol) was added in four portions with 5 min interval. Then, the reaction was continued for 4 h at the same temperature and the solution was poured into crushed ice slowly, followed by basification with Na_2CO_3. The solution was extracted with EtOAc twice (2 × 100 mL) and the combined organic layer was washed with water. The solvent was evaporated under reduced pressure and then purified by a silica gel column (hexane/ethyl acetate (1:5)) to afford dibromo compound DBBPy with 82% yield. ^{1}H NMR (400 MHz, $CDCl_3$): δ 8.83−8.80 (m, 2 H), 7.57−7.55 (m, 2 H), 7.51−7.50 (m, 2 H), 7.47 (d, J = 1.4 Hz, 1 H). HRMS (EI, m/z): [M^+] cal for $C_{12}H_7Br_2NO$ 338.8894, found 338.8891.

Synthesis of DCBPy. To an oven-dried seal tube (2,5-dibromophenyl) (pyridine-4-yl)methanone (DBBPy) (2.50 g, 7.33 mmol), carbazole (3.06 g, 18.3 mmol), Cu (0.93 g, 14.7 mmol), K_2CO_3 (5.06 g, 36.7 mmol) and 1,2-dichlorobenzene (20 mL) was added. The system was evacuated and purged with nitrogen three times and the mixture was heated and stirred at 180 °C for 48 h. The reaction mixture was filtered through Celite and washed with ethyl acetate (30 mL). Solvent was evaporated under reduced pressure and then purified by column chromatography (hexane/ethyl acetate (4:1)) to afford the desired yellow solid (DCBPy) in 57% yield.

Yellow solid; mp 130 °C: ^{1}H NMR (400 MHz, $CDCl_3$): δ 8.21 (sd, J = 2.4 Hz, 1 H), 8.19 (d, J = 7.6 Hz, 2 H), 8.09 (dd, J = 8.4 Hz, J = 1.6 Hz, 1 H), 7.92−7.90 (m, 3 H), 7.83 (d, J = 7.6 Hz, 2 H), 7.65 (d, J = 8.4 Hz, 2 H), 7.53−7.49 (m, 2 H), 7.45−7.41 (m, 2 H), 7.38 (m, 4 H), 7.23 (t, J = 7.6 Hz, 2 H), 6.68 (dd, J = 8.4 Hz, J = 1.6 Hz, 2 H); ^{13}C NMR (100 MHz, $CDCl_3$): δ 194.96 (*C*O), 148.78 (2 *C*H), 142.07 (*C*), 140.51 (2 *C*), 140.21 (2 *C*), 138.07 (*C*), 137.21 (*C*), 134.82 (*C*), 131.47 (*C*H), 130.46 (*C*H), 129.31 (*C*H), 126.35 (2 *C*H), 126.16 (2 *C*H), 123.84 (2 *C*), 123.19 (2 *C*), 120.81 (2 *C*H), 120.77 (2 *C*H), 120.60 (2 *C*H), 120.38 (2 *C*H), 119.90 (2 *C*H), 109.53 (4 *C*H); HRMS (EI, m/z): [M^+] cal for $C_{36}H_{23}N_3O$ 513.1841, found 513.1837.

Synthesis of DTCBPy. A procedure similar to the synthesis of DCBPy was used for the synthesis of DTCBPy using DBBPy (2.50 g, 7.33 mmol), 3,6-di-*tert*-butyl-9*H*-carbazole (5.11 g, 18.3 mmol), Cu (0.93 g, 14.7 mmol), K_2CO_3 (5.06 g, 36.7 mmol) and 1,2-dichlorobenzene (20 mL) in 61% yield.

Yellow solid; mp 306 °C: ^{1}H NMR (400 MHz, $CDCl_3$): δ 8.17 (s, 3 H), 8.06 (dd, J = 8.4 Hz, J = 2.4 Hz, 1 H), 7.88 (s, 1 H), 7.87−7.85 (m, 2 H), 7.81−7.80 (m, 2 H), 7.59−7.53 (m, 4 H), 7.47 (dd, J = 8.8 Hz, J = 2.0 Hz, 2 H), 7.25 (d, J = 8.8 Hz, 2 H), 6.65−6.63 (m, 2 H), 1.49 (s, 18 H), 1.44 (s, 18 H); ^{13}C NMR (100 MHz, $CDCl_3$): δ 194.95 (*C*O), 148.63 (2 *C*H), 143.84 (2 *C*), 143.79 (2 *C*), 142.03 (*C*), 139.22 (2 *C*), 138.67 (2 *C*), 138.23 (*C*), 136.59 (*C*), 135.01 (*C*), 130.95 (*C*H), 130.13 (*C*H), 128.97 (*C*H), 123.98 (2 *C*H), 123.89 (2 *C*), 123.76 (2 *C*H), 123.38 (2 *C*), 119.92 (2 *C*H), 116.53 (2 *C*H), 116.36 (2 *C*H), 109.07 (4 *C*H), 34.79 (2 *C*), 34.73 (2 *C*), 31.97 (6 *C*H$_3$), 31.95 (6 *C*H$_3$). HRMS (EI, m/z): [M^+] cal for $C_{52}H_{55}N_3O$ 737.4345, found 737.4338.

ASSOCIATED CONTENT

Supporting Information

The Supporting Information is available free of charge on the ACS Publications website at DOI: 10.1021/jacs.5b10950.

General information, computational details, UV−vis, Pl, CV, TGA, DSC, Luminance vs power efficiency and current efficiency, and EL spectra. (PDF)

Crystal data. (CIF)

AUTHOR INFORMATION

Corresponding Author

*chcheng@mx.nthu.edu.tw

Notes

The authors declare no competing financial interest.

ACKNOWLEDGMENTS

We thank the Ministry of Science and Technology of Republic of China (MOST 103-2633-M-007-001) for support of this research and the National Center for High-Performance Computing (Account number: u32chc04) of Taiwan for providing the computing time.

REFERENCES

(1) *Organic Light-Emitting Devices: Synthesis Properties and Applications*; Müllen, K., Scherf, U., Eds.; Wiley-VCH: Weinheim, 2006.

(2) *Highly Efficient OLEDs with Phosphorescent Materials*; Yersin, H., Ed.; Wiley-VCH: Weinheim, 2008.

(3) Farinola, G. M.; Ragni, R. *Chem. Soc. Rev.* **2011**, *40*, 3467−3482.

(4) Schwartz, G.; Pfeiffer, M.; Reineke, S.; Walzer, K.; Leo, K. *Adv. Mater.* **2007**, *19*, 3672−3676.

(5) Chou, H.-H.; Chen, Y.-H.; Hsu, H.-P.; Chang, W.-H.; Chen, Y.-H.; Cheng, C.-H. *Adv. Mater.* **2012**, *24*, 5867−5871.

(6) Lee, C. W.; Lee, J. Y. *Adv. Mater.* **2013**, *25*, 5450−5454.

(7) Gather, M. C.; Kçhnen, A.; Meerholz, K. *Adv. Mater.* **2011**, *23*, 233−248.

(8) Kamtekar, K. T.; Monkman, A. P.; Bryce, M. R. *Adv. Mater.* **2010**, *22*, 572−582.

(9) Sun, N.; Wang, Q.; Zhao, Y.; Chen, Y.; Yang, D.; Zhao, F.; Chen, J.; Ma, D. *Adv. Mater.* **2014**, *26*, 1617−1621.

(10) Reineke, S.; Rosenow, T. C.; Lüssem, B.; Leo, K. *Adv. Mater.* **2010**, *22*, 3189−3193.

(11) Wu, K.-C.; Ku, P.-J.; Lin, C.-S.; Shih, H.-T.; Wu, F.-I.; Huang, M.-J.; Lin, J.-J.; Chen, I.-C.; Cheng, C.-H. *Adv. Funct. Mater.* **2008**, *18*, 67−75.

(12) Schwartz, G.; Reineke, S.; Rosenow, T. C.; Walzer, K.; Leo, K. *Adv. Funct. Mater.* **2009**, *19*, 1319−1333.

DOI: 10.1021/jacs.5b10950
J. Am. Chem. Soc. 2016, 138, 628−634

(13) Reineke, S.; Lindner, F.; Schwartz, G.; Seidler, N.; Walzer, K.; Lüssem, B.; Leo, K. *Nature* **2009**, *459*, 234−238.
(14) Baldo, M. A.; Thompson, M. E.; Forrest, S. R. *Nature* **2000**, *403*, 750−753.
(15) Lu, K.-Y.; Chou, H.-H.; Hsieh, C.-H.; Yang, Y.-H. O.; Tsai, H.-R.; Tsai, H.-Y.; Hsu, L.-C.; Chen, C.-Y.; Chen, I.-C.; Cheng, C.-H. *Adv. Mater.* **2011**, *23*, 4933−4937.
(16) Fan, C.; Zhu, L.; Liu, T.; Jiang, B.; Ma, D.; Qin, J.; Yang, C. *Angew. Chem., Int. Ed.* **2014**, *53*, 2147−2151.
(17) Du, B.-S.; Liao, J.-L.; Huang, M.-H.; Lin, C.-H.; Lin, H.-W.; Chi, Y.; Fan, G.-L.; Wong, K.-T.; Lee, G.-H.; Chou, P.-T. *Adv. Funct. Mater.* **2012**, *22*, 3491−3499.
(18) Lin, S.-H.; Wu, F.-I.; Tsai, H.-Y.; Chou, P.-Y.; Chou, H.-H.; Cheng, C.-H.; Liu, R.-S. *J. Mater. Chem.* **2011**, *21*, 8122−8128.
(19) Adachi, C.; Baldo, M. A.; Thompson, M. E.; Forrest, S. R. *J. Appl. Phys.* **2001**, *90*, 5048−5051.
(20) Ganzorig, C.; Fujihira, M. *Appl. Phys. Lett.* **2002**, *81*, 3137−3139.
(21) Zhang, D.; Duan, L.; Li, C.; Li, Y.; Li, H.; Zhang, D.; Qiu, Y. *Adv. Mater.* **2014**, *26*, 5050−5055.
(22) Chou, P.-Y.; Chou, H.-H.; Chen, Y.-H.; Su, T.-H.; Liao, C.-Y.; Lin, H.-W.; Lin, W.-C.; Yen, H.-Y.; Chen, I.-C.; Cheng, C.-H. *Chem. Commun.* **2014**, *50*, 6869−6871.
(23) Wang, Q.; Oswald, I. W. H.; Perez, M. R.; Jia, H.; Gnade, B. E.; Omary, M. A. *Adv. Funct. Mater.* **2013**, *23*, 5420−5428.
(24) Chiang, C. J.; Kimyonok, A.; Etherington, M. K.; Griffiths, G. C.; Jankus, V.; Turksoy, F.; Monkman, A. P. *Adv. Funct. Mater.* **2013**, *23*, 739−746.
(25) Zhang, Q.; Komino, T.; Huang, S.; Matsunami, S.; Goushi, K.; Adachi, C. *Adv. Funct. Mater.* **2012**, *22*, 2327−2336.
(26) Komino, T.; Nomura, H.; Koyanagi, T.; Adachi, C. *Chem. Mater.* **2013**, *25*, 3038−3047.
(27) Méhes, G.; Nomura, H.; Zhang, Q.; Nakagawa, T.; Adachi, C. *Angew. Chem., Int. Ed.* **2012**, *51*, 11311−11315.
(28) Li, J.; Nakagawa, T.; MacDonald, J.; Zhang, Q.; Nomura, H.; Miyazaki, H.; Adachi, C. *Adv. Mater.* **2013**, *25*, 3319−3323.
(29) Tao, Y.; Yuan, K.; Chen, T.; Xu, P.; Li, H.; Chen, R.; Zheng, C.; Zhang, L.; Huang, W. *Adv. Mater.* **2014**, *26*, 7931−7958.
(30) Cui, L.-S.; Xie, Y.-M.; Wang, Y.-K.; Zhong, C.; Deng, Y.-L.; Liu, X.-Y.; Jiang, Z.-Q.; Liao, L.-S. *Adv. Mater.* **2015**, *27*, 4213−4217.
(31) Sun, J. W.; Lee, J.-H.; Moon, C.-K.; Kim, K.-H.; Shin, H.; Kim, J.-J. *Adv. Mater.* **2014**, *26*, 5684−5688.
(32) Kim, M.; Jeon, S. K.; Hwang, S.-H.; Lee, J. Y. *Adv. Mater.* **2015**, *27*, 2515−2520.
(33) Zhang, Q.; Li, B.; Huang, S.; Nomura, H.; Tanaka, H.; Adachi, C. *Nat. Photonics* **2014**, *8*, 332−338.
(34) Hirata, S.; Sakai, Y.; Masui, K.; Tanaka, H.; Lee, S. Y.; Nomura, H.; Nakamura, N.; Yasumatsu, M.; Nakanotani, H.; Zhang, Q.; Shizu, K.; Miyazaki, H.; Adachi, C. *Nat. Mater.* **2015**, *14*, 330−336.
(35) Goushi, K.; Yoshida, K.; Sato, K.; Adachi, C. *Nat. Photonics* **2012**, *6*, 253−258.
(36) Shizu, K.; Tanaka, H.; Uejima, M.; Sato, T.; Tanaka, K.; Kaji, H.; Adachi, C. *J. Phys. Chem. C* **2015**, *119*, 1291−1297.
(37) Zhang, Q.; Kuwabara, H.; Potscavage, W. J.; Huang, S.; Hatae, Y.; Shibata, T.; Adachi, C. *J. Am. Chem. Soc.* **2014**, *136*, 18070−18081.
(38) Tsai, W.-L.; Huang, M.-H.; Lee, W.-K.; Hsu, Y.-J.; Pan, K.-C.; Huang, Y.-H.; Ting, H.-C.; Sarma, M.; Ho, Y.-Y.; Hu, H.-C.; Chen, C.-C.; Lee, M.-T.; Wong, K.-T.; Wu, C.-C. *Chem. Commun.* **2015**, *51*, 13662.
(39) Zhang, Q.; Tsang, D.; Kuwabara, H.; Hatae, Y.; Li, B.; Takahashi, T.; Lee, S. Y.; Yasuda, T.; Adachi, C. *Adv. Mater.* **2015**, *27*, 2096−2100.
(40) Kawasumi, K.; Wu, T.; Zhu, T.; Chae, H. S.; Voorhis, T. V.; Baldo, M. A.; Swager, T. M. *J. Am. Chem. Soc.* **2015**, *137*, 11908−11911.
(41) Lin, N.; Qiao, J.; Duan, L.; Li, H.; Wang, L.; Qiu, Y. *J. Phys. Chem. C* **2012**, *116*, 19451−19457.
(42) Lin, N.; Qiao, J.; Duan, L.; Wang, L.; Qiu, Y. *J. Phys. Chem. C* **2014**, *118*, 7569−7578.
(43) Tanaka, H.; Shizu, K.; Miyazaki, H.; Adachi, C. *Chem. Commun.* **2012**, *48*, 11392−11394.
(44) Hong, Y.; Lam, J. W. Y.; Tang, B. Z. *Chem. Commun.* **2009**, 4332−4353.
(45) Uoyama, H.; Goushi, K.; Shizu, K.; Nomura, H.; Adachi, C. *Nature* **2012**, *492*, 234−238.
(46) Lee, C. W.; Lee, J. Y. *Chem. Mater.* **2014**, *26*, 1616−1621.
(47) Su, S.-J.; Chiba, T.; Takeda, T.; Kido, J. *Adv. Mater.* **2008**, *20*, 2125−2130.
(48) Zhang, Q.; Li, J.; Shizu, K.; Huang, S.; Hirata, S.; Miyazaki, H.; Adachi, C. *J. Am. Chem. Soc.* **2012**, *134*, 14706−14709.
(49) Shih, C.-H.; Rajamalli, P.; Wu, C.-A.; Chiu, M.-J.; Chu, L.-K.; Cheng, C.-H. *J. Mater. Chem. C* **2015**, *3*, 1491−1496.
(50) Chou, H.-H.; Cheng, C.-H. *Adv. Mater.* **2010**, *22*, 2468−2471.
(51) Su, S.-J.; Chiba, T.; Takeda, T.; Kido, J. *Adv. Mater.* **2008**, *20*, 2125.

DOI: 10.1021/jacs.5b10950
J. Am. Chem. Soc. 2016, 138, 628−634